



Supplement of

Multi-scale soil moisture data and process-based modeling reveal the importance of lateral groundwater flow in a subarctic catchment

Jari-Pekka Nousu et al.

Correspondence to: Jari-Pekka Nousu (jari-pekka.nousu@luke.fi)

The copyright of individual parts of the supplement might differ from the article licence.

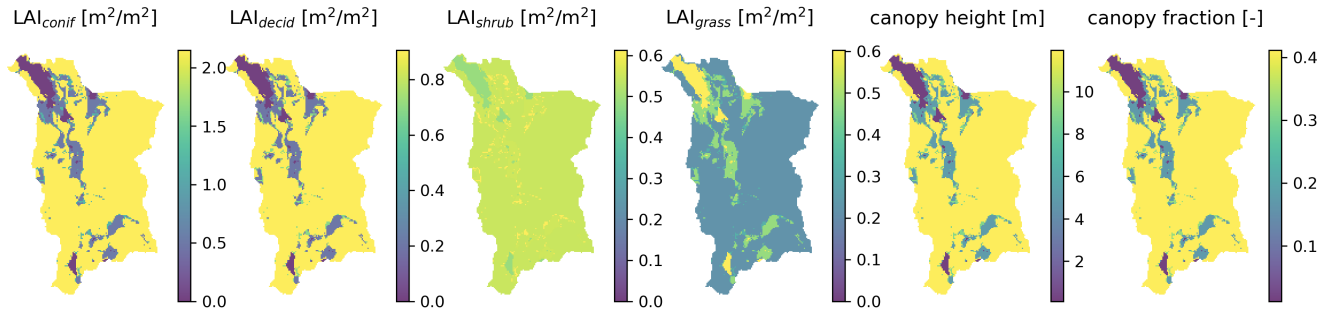


Figure S1. Site averaged vegetation GIS rasters.

Table S1. Site type-specific organic moss-humus layer hydraulic parameters. The $\theta_{s,org}$, $\theta_{fc,org}$ and $\theta_{wp,org}$ are porosity, field capacity and wilting point, respectively. $K_{sat,org}$ is saturated hydraulic conductivity and β_{org} is a parameter describing power-law decay of hydraulic conductivity with decreasing saturation ratio.

Site	$\theta_{s,org}$ ($\text{m}^3 \text{m}^{-3}$)	$\theta_{fc,org}$ ($\text{m}^3 \text{m}^{-3}$)	$\theta_{wp,org}$ ($\text{m}^3 \text{m}^{-3}$)	$K_{sat,org}$ (m s^{-1})	β_{org} (-)	Source
Mineral	0.90	0.30	0.20	$1 \cdot 10^{-3}$	6.0	Williams and Flanagan (1996); Elumeeva et al. (2011)
Spruce mire	0.90	0.65	0.30	$1 \cdot 10^{-3}$	6.0	Williams and Flanagan (1996); Elumeeva et al. (2011)
Pine mire	0.90	0.65	0.30	$1 \cdot 10^{-3}$	6.0	Williams and Flanagan (1996); Elumeeva et al. (2011)
Treeless mire	0.90	0.65	0.30	$1 \cdot 10^{-3}$	6.0	Williams and Flanagan (1996); Elumeeva et al. (2011)

Table S2. Soil type-specific rootzone layer hydraulic parameters. The $\theta_{s,root}$, $\theta_{fc,root}$ and $\theta_{wp,root}$ are porosity, field capacity and wilting point, respectively. $K_{sat,root}$ is saturated hydraulic conductivity and β_{root} is a parameter describing power-law decay of hydraulic conductivity with decreasing saturation ratio.

Soil texture	$\theta_{s,root}$ ($\text{m}^3 \text{m}^{-3}$)	$\theta_{fc,root}$ ($\text{m}^3 \text{m}^{-3}$)	$\theta_{wp,root}$ ($\text{m}^3 \text{m}^{-3}$)	$K_{sat,root}$ (m s^{-1})	β_{root} (-)	Source
Coarse	0.41	0.21	0.10	$1 \cdot 10^{-4}$	3.1	Launiainen et al. (2019)
Medium	0.43	0.33	0.13	$1 \cdot 10^{-5}$	4.7	Launiainen et al. (2019)
Peat	0.89	0.53	0.36	$3 \cdot 10^{-4}$	6.0	Autio et al. (2023)

Table S3. Soil type-specific deep layer parameters. The $\theta_{s,deep}$ and $\theta_{r,deep}$ are porosity and residual water content parameter, respectively. The α and n are van Genuchten-Mualem fitting parameters (van Genuchten, 1980). The $K_{sat,root}$ is saturated hydraulic conductivity.

Soil texture	$\theta_{s,deep}$ ($\text{m}^3 \text{m}^{-3}$)	$\theta_{r,deep}$ ($\text{m}^3 \text{m}^{-3}$)	α (-)	n (-)	$K_{sat,deep}$ (m s^{-1})	Source
Coarse	0.41	0.05	0.024	1.20	$1 \cdot 10^{-5}$	Launiainen et al. (2019)
Medium	0.43	0.05	0.024	1.20	$1 \cdot 10^{-5}$	Launiainen et al. (2019)
Peat	0.89	0.20	0.072	1.26	$1 \cdot 10^{-5}$	Autio et al. (2023)

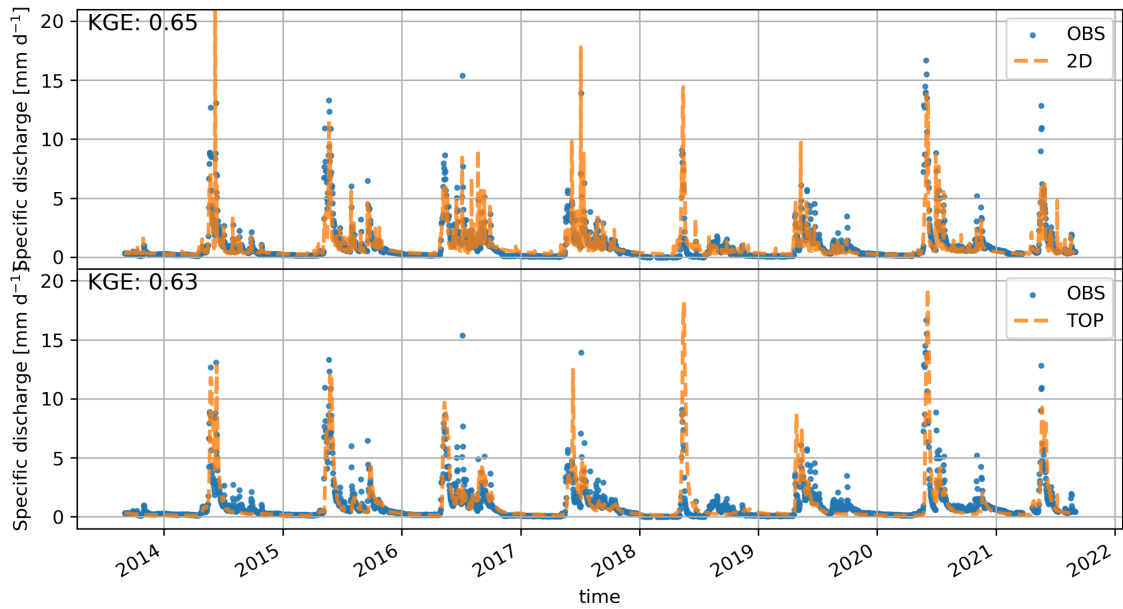


Figure S2. Comparison of specific discharges simulated by 2D (upper row) and TOP (lower row) conceptualizations against observations. Some observations are missing between April and June in 2018. KGE refers to the Kling-Gupta Efficiency (Gupta et al., 2009).

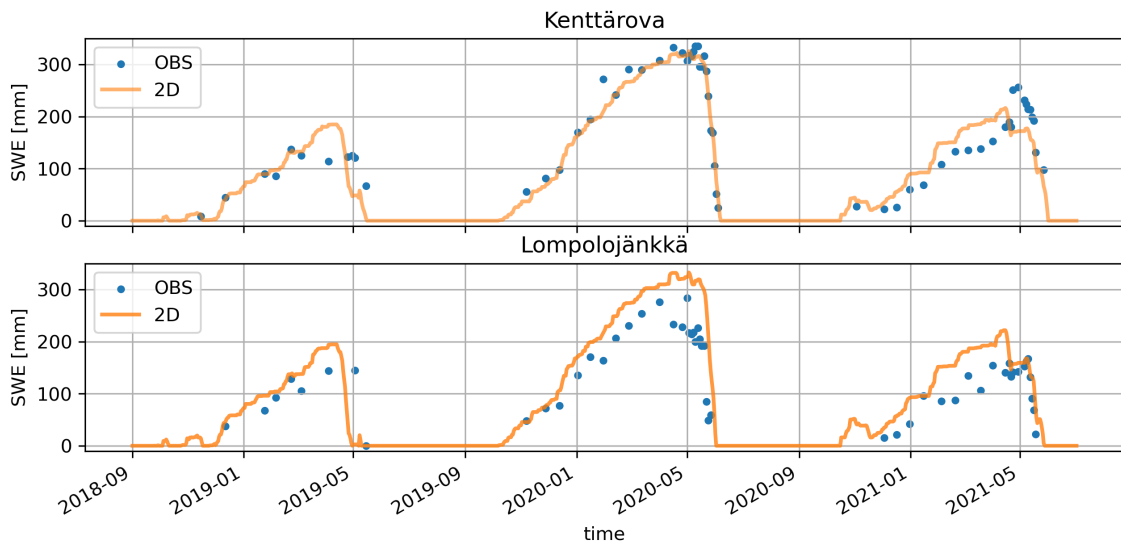


Figure S3. Comparison of simulated and observed snow water equivalent (SWE) from 2018 autumn to 2021 summer at Kenttäröva and Lompolojänkkä sites.

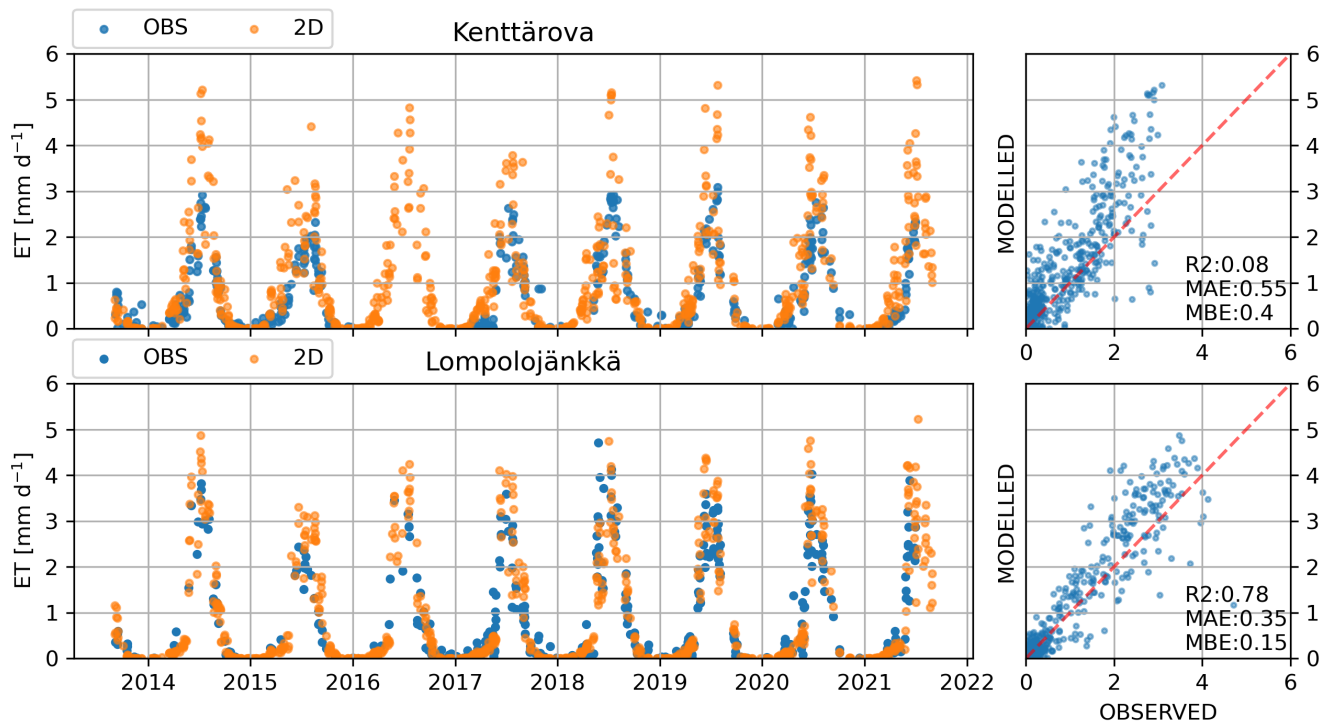


Figure S4. Comparison of simulated and observed evapotranspiration (ET) at Kenttäröva and Lompolojänkkä sites. Only dry-canopy conditions (i.e. no precipitation during the current or previous day), and days with more than 90 % available hourly ET observations were considered.

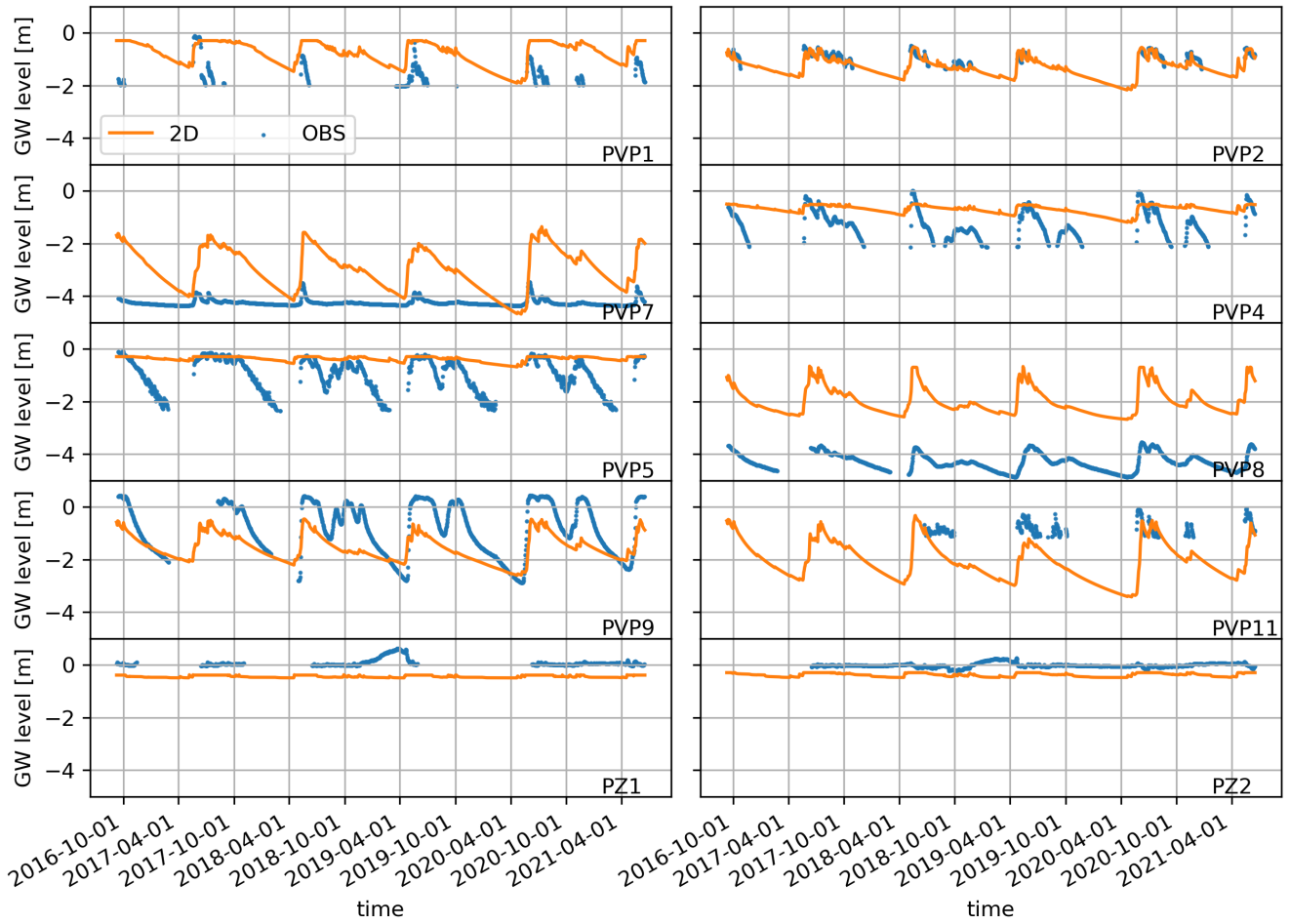


Figure S5. Temporal dynamics of 2D simulated and in-situ measured groundwater levels at 10 different locations around the catchment.

Table S4. Performance metrics of 2D simulated and in-situ measured groundwater levels at 10 different locations around the catchment.

Location	Mean biased error (m)	Mean absolute error (m)
PVP1	1.04	1.07
PVP2	-0.08	0.15
PVP4	0.62	0.67
PVP5	0.61	0.63
PVP7	1.27	1.29
PVP8	2.34	2.34
PVP9	-0.70	0.79
PVP11	-0.81	0.86
PZ1	-0.51	0.51
PZ2	-0.37	0.37
MEAN	0.34	0.87

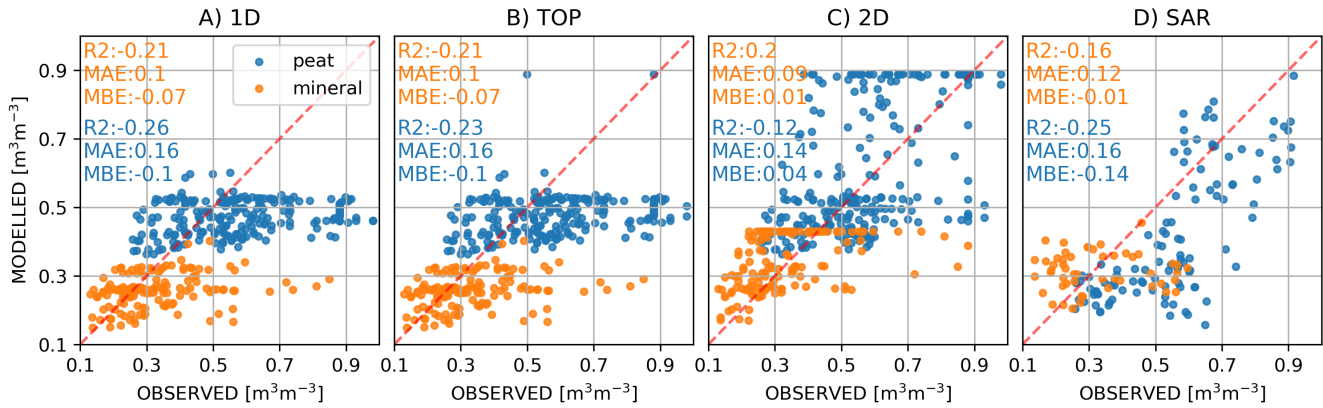


Figure S6. Comparison of simulated rootzone soil moisture content and SAR-based surface soil moisture estimates against spatiotemporal manual in-situ soil moisture observations. The blue color of the points correspond to peat soil and the orange color to mineral soil.

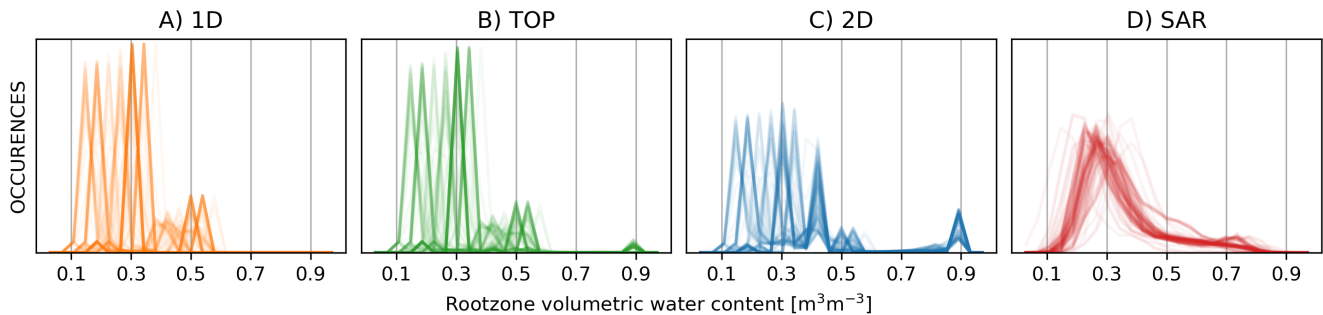


Figure S7. Daily distributions of simulated rootzone soil moisture (1D, TOP and 2D) and SAR-based surface soil moisture.

Table S5. Statistics of SpaFHy-1D, SpaFHy-TOP, SpaFHy-2D and SAR morning estimates. Low and high soil moisture quantiles are represented as $q = 0.1$ and $q = 0.9$, respectively. All statistics were calculated for those days when SAR morning estimates were available.

Data	mean ($\text{m}^3 \text{m}^{-3}$)	variance ($\text{m}^3 \text{m}^{-3}$)	$q = 0.1$ ($\text{m}^3 \text{m}^{-3}$)	$q = 0.9$ ($\text{m}^3 \text{m}^{-3}$)
SpaFHy-1D	0.29	0.01	0.25	0.47
SpaFHy-TOP	0.30	0.01	0.25	0.47
SpaFHy-2D	0.39	0.04	0.25	0.82
SAR	0.34	0.02	0.22	0.65

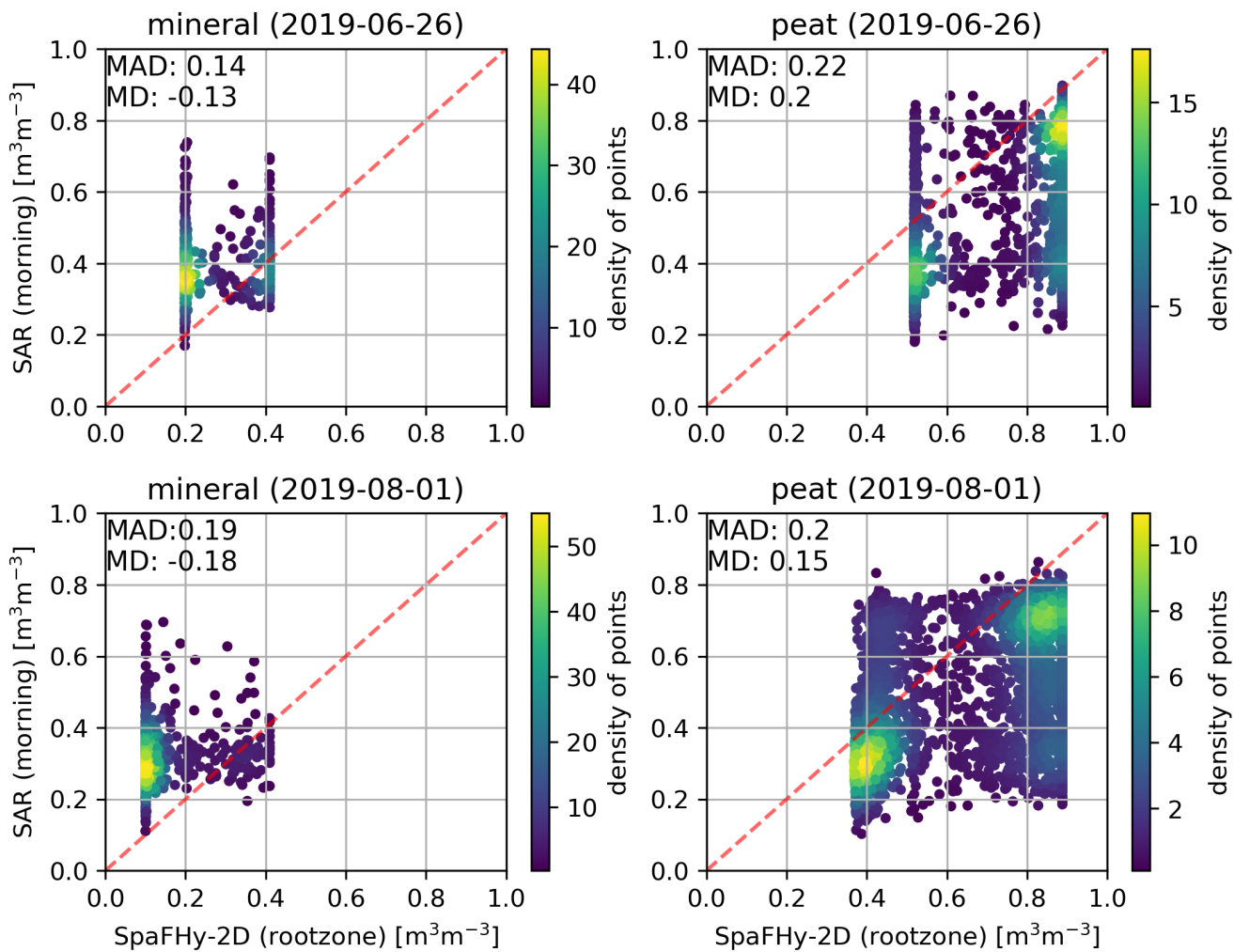


Figure S8. Density scatterplots of SpaFH2D vs. SAR on mineral (left column) and peat (right column) soil on 2019-06-26 (first row) and 2019-08-01 (second row). Mean absolute difference (MAD) and mean difference (MD) are presented in each panel.

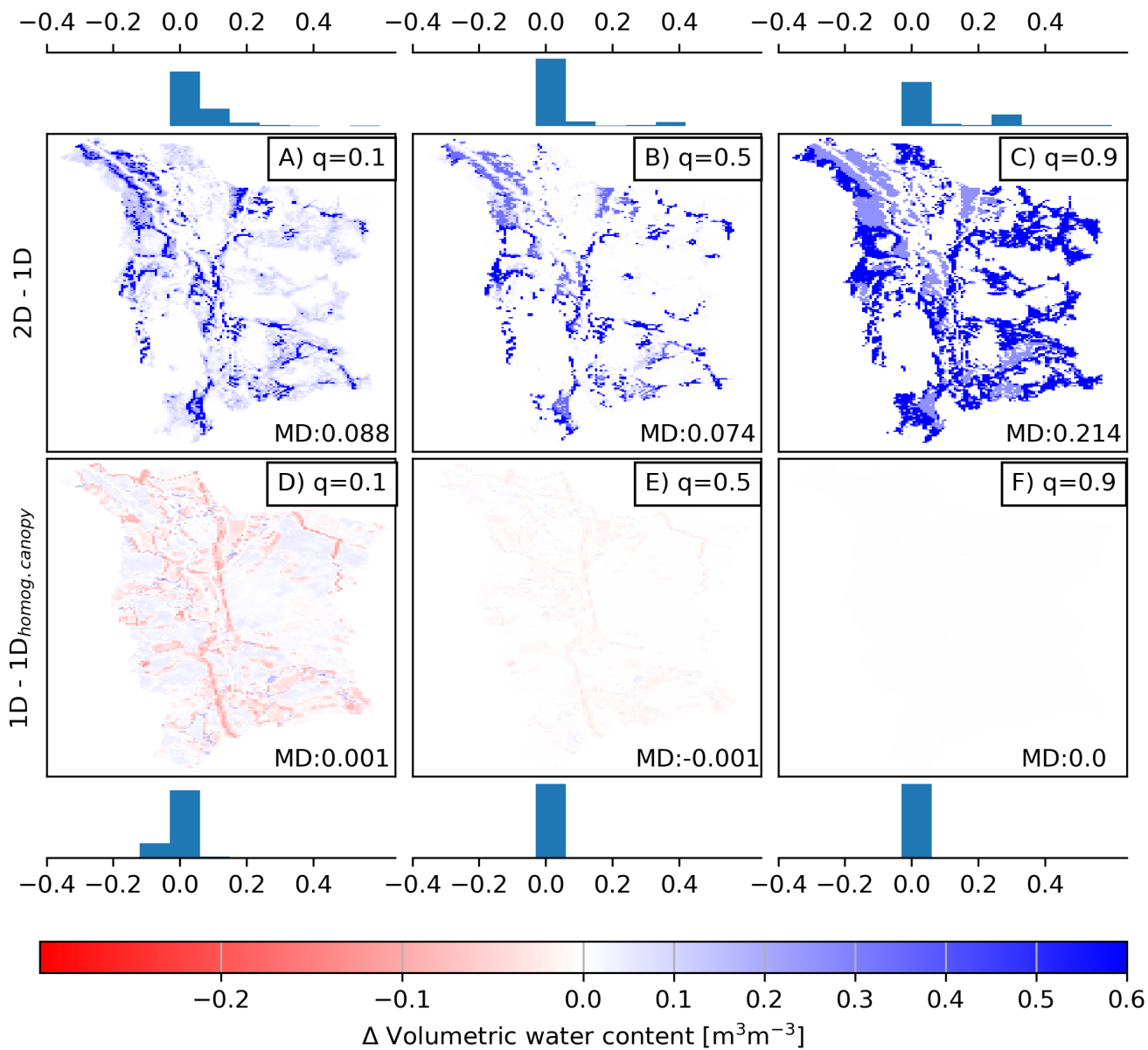


Figure S9. The impact of lateral groundwater flow (upper row) on organic moss-humus layer soil moisture expressed as $\Delta = 2D - 1D$, and the impact of vegetation heterogeneity (bottom row) expressed as $\Delta = 1D - 1D_{homog.canopy}$ in different catchment soil moisture states. The panels correspond to 0.1, 0.5, and 0.9 quantiles of grid-cell soil moisture, and the bars show distribution of binned differences. Mean difference (MD) is shown in each panel.

References

- Autio, A., Ala-Aho, P., Rossi, P. M., Ronkanen, A.-K., Aurela, M., Lohila, A., Korpelainen, P., Kumpula, T., Klöve, B., and Marttila, H.: Groundwater exfiltration pattern determination in the sub-arctic catchment using thermal imaging, stable water isotopes and fully-integrated groundwater-surface water modelling, *Journal of Hydrology*, 626, 130342, <https://doi.org/https://doi.org/10.1016/j.jhydrol.2023.130342>, 2023.
- 5 Elumeeva, T. G., Soudzilovskaia, N. A., Doring, H. J., and Cornelissen, J. H.: The importance of colony structure versus shoot morphology for the water balance of 22 subarctic bryophyte species, *Journal of Vegetation Science*, 22, 152–164, <https://doi.org/10.1111/j.1654-1103.2010.01237.x>, 2011.
- Gupta, H. V., Kling, H., Yilmaz, K. K., and Martinez, G. F.: Decomposition of the mean squared error and NSE performance criteria: Implications for improving hydrological modelling, *Journal of Hydrology*, 377, 80–91, <https://doi.org/https://doi.org/10.1016/j.jhydrol.2009.08.003>, 2009.
- 10 Launiainen, S., Guan, M., Salmivaara, A., and Kieloaho, A. J.: Modeling boreal forest evapotranspiration and water balance at stand and catchment scales: a spatial approach, *Hydrology and Earth System Sciences*, 23, 3457–3480, <https://doi.org/10.5194/hess-23-3457-2019>, 2019.
- 15 van Genuchten, M. T.: A Closed-form Equation for Predicting the Hydraulic Conductivity of Unsaturated Soils, *Soil Science Society of America Journal*, 44, 892–898, <https://doi.org/10.2136/sssaj1980.03615995004400050002x>, 1980.
- Williams, T. G. and Flanagan, L. B.: Effect of changes in water content on photosynthesis, transpiration and discrimination against ^{13}C and $\text{C}^{18}\text{O}^{16}\text{O}$ in *Pleurozium* and *Sphagnum*, *Oecologia*, 108, 38–46, <https://doi.org/10.1007/BF00333212>, 1996.